Investigations on conductivity of nitrogen-doped reduced graphene oxide/Li_2FeSiO_4 cathode material prepared by microwave-assisted method for lithium-ion batteries

Saba Zomorrodi[1], Pirooz Marashi[2*], Zahra Sadeghian[3], Soheila Javadian[4]

[1]PhD candidate, Department of Materials Science and Metallurgical Engineering, Amirkabir University of Technology, Tehran, Iran

[2]Associate professor, Department of Materials Science and Metallurgical Engineering, Amirkabir University of Technology, Tehran, Iran, pmarashi@aut.ac.ir

[3]Associate professor, Research Institute of Petroleum Industry (RIPI), Tehran, Iran

[4]Associate professor, Faculty of Basic Science, Tarbiat Modares University, Tehran, Iran

Abstract:

Li_2FeSi0_4 is a promising cathode active material for lithium-ion batteries due to its significant theoretical capacity (332 $mAhg^{-1}$). Nevertheless, its practical electrochemical performance faces significant hurdles due to low electron conductivity. In the research, a simple solid-state technique was used to synthesize the high-purity cathode material Li_2FeSi0_4. Additionally, nitrogen-doped reduced graphene oxide nanosheets were fabricated using a household microwave-assisted process and then selectively deposited to coat the active cathode material to increase conductivity and significantly improve electrocatalysis. The properties of the as-prepared nanosheets and Li_2FeSi0_4/ nitrogen-doped reduced graphene oxide nanocomposites are studied using X-ray diffraction, high resolution transmission electron microscopy, field emission scanning electron microscopy, RAMAN spectrometry and Fourier transform infrared spectroscopy techniques. The study investigated the influence of different amounts of as-prepared nanosheets coatings on the electrical conductivity of the Li_2FeSi0_4 by comparing their band gap energy value. Accordingly, lower band gap, indicating higher and better electronic conductivity in the cathode of lithium-ion batteries. Therefore, diffusion reflectance spectroscopy and electrochemical impedance spectroscopy were used to determine the band gap size and conductivity. Studies show that coating Li_2FeSi0_4 particles with only 5 wt% nitrogen-doped nanosheets reduced the bandgap energy value by about 0.78 eV and increased the electrical conductivity by 54.31%. It is concluded that Li_2FeSi0_4/ nitrogen-doped reduced graphene oxide

nanocomposites can be a promising candidate as a high-performance cathode material for lithium-ion batteries.

Keywords:

lithium iron orthosilicate, graphene nanosheets, solid-state synthesis, bandgap, LIBs

1. The introduction

With the advancement of society and the continuous progress in science and technology, great emphasis is placed on new energy sources for sustainable development. Research into Li-ion energy batteries has been a topic of interest for years [1]. Three commercially successful cathode materials for Li-ion batteries have emerged: Li_2MnO_4, $LiCoO_2$, and $LiNiO_2$. However, ongoing research is dedicated to finding alternatives that are less toxic, less expensive, more stable, and safer. Polyanionic Li-ion cathode materials such as LiMPO (M=Fe, Co, Mn, Ni) offer advantages such as affordability, high safety, good chemical and thermal stability and lower environmental impact [2, 3]. Among these materials, $LiFePO_4$ (LFP) has found successful applications in electric vehicles thanks to its robust covalent P-O band, which significantly increases stability. However, the performance of such materials is significantly influenced by manufacturing conditions, which introduce challenges such as poor electronic and ionic conductivity, low cycling performance, and the need for increased battery capacity. The continuous search for a cathode material that is both cost-effective and stable and whose properties meet acceptable standards has attracted considerable attention in the exploration of silicate structure alternatives within the Li-Fe-Si-O combination [4, 5]. Nyten [6] proposed Li_2FeSiO_4 (LFS) as a potential cathode material for Li-ion batteries, offering twice the capacity of $LiFePO_4$ (332 $mAhg^{-1}$) if both Li-ions could actively participate in the reaction [7, 8]. The expected advantages include the reduction of the deintercalation voltage for the formation of the Fe^{3+}-Fe^{2+} redox couple due to the lower electronegativity of Si (2.03) compared to P (2.39) [9, 10]. In addition, there is a difference in the band gap, i.e., the gap between the lower Fermi level of the valence band and the upper Fermi level of the conduction band. This gap is smaller for LFS than for LFP (4 eV). The results

indicate that the electronic conductivity in LFS exceeds that in LFP. This difference is attributed to the smaller band gap, indicating better electronic conductivity in the electrode of lithium-ion batteries (LIBs) [11]. Nevertheless, its practical electrochemical performance faces significant hurdles due to low electron conductivity and slow Li^+ diffusion. To address problems such as poor electrical conductivity ($\sim 10^{-15}$ $S \cdot cm^{-1}$) and sluggish Li-ion motion in LFS, scientists found solutions through size reduction, coating with conductive materials, nanostructure design, and ion doping [12, 13]. Reducing the particle size improves ionic conductivity, shorten the Li-ion travel distance, improve the contact with the electrolyte, increase more interaction that results in higher electron transport. The tailored particle size increases the specific surface area and provides an abundance of active sites that facilitate charge transfer reactions. Therefore, effective charge carrier transport prevents ion and electron losses and thus enables rapid ion and electron migration. This results in larger specific capacity and improved cycling performance [14, 15]. Applying a surface coating is a widely used technique to control side reactions and increase the conductivity of cathode materials. Improving the electrochemical performance of LFS is achieved through conductive material coatings in which carbon plays the main role. This coating not only avoids some side reactions with the electrolyte but combination with the nano size it also shortens the distance traveled by the Li-ion, thus increasing both ionic conductivity and diffusivity. Carbon nanotubes, graphene oxide (GO) and rGO, known for their impressive electrical conductivity, are widely used as coatings for LFS [16, 17]. Multiple performance evaluations of composite – some containing rGO, others without rGO and with 2D or 3D frameworks – show that 3D-G LFS/C has increased capacity and improved cycling stability. The practical connection between rGO nanosheets and LFS/C nanoparticles minimizes contact resistance, ensures a strong band, and improves cycling performance. Furthermore, the conductive network constructed by rGO nanosheets in the composite creates a three-dimensional path for electron migration during charging and discharging [18-21]. rGO presents a challenge in composite integration with other materials because it does not have a band gap. Researchers find the modification of rGO fascinating. This change is divided into physical and chemical methods, with the latter being the more common choice. Introducing other atoms into rGO through chemical doping is an effective strategy to open its band gap and expand its applicability

in various nanodevices [22, 23]. Recently, doping with heteroatoms (particularly N) has proven effective in improving the electrical properties of carbon-based materials. Due to the similar atomic radius of N and C, the easy incorporation of N atoms into the carbon matrix facilitates this process. Introducing more electron-rich N into the carbon network channels additional electrons into the delocalized p-system of carbon materials, thereby increasing electrical conductivity [24, 25]. Moreover, the pronounced electronegativity of N and C significantly influences the charge distribution of C atoms, forming numerous active sites and vacancies or intrinsic defects in the carbon structure [22, 26]. These additional defects serve as pathways for the diffusion of Li-ions and electrolytes and play a crucial role in Li-ion or Na-ion batteries. At the same time, the rate capability is significantly improved and the impedance is reduced. Surprisingly, there are hardly any reports on nitrogen-doped carbon-coated LFS [27, 28]. While previous studies involved the time- and energy-intensive synthesis of N-rGO, the microwave-assisted heating technique emerges as a rapid and straightforward method for producing advanced materials in inorganic synthesis. This approach not only proves to be extremely efficient in terms of energy consumption, but is also characterized by its environmental friendliness. Unlike traditional heating methods, microwave heating achieves rapid and uniform heating by utilizing self-heating processes and absorbing microwave energy directly into the materials [29]. In this study, high-purity LFS cathode material was synthesized by a simple solid-state process and coated with N-rGO nanosheets fabricated by a microwave-assisted method. The influence of N-rGO coating on the electrical conductivity of the cathode material of LIBs was investigated by comparing their bandgap energy values.

2. Experimental

2-1- Preparation of N-rGO

In the first step, GO was synthesized from expanded graphite flakes using a modified Hummers method. All material is used as received without further purification. 180 ml of sulfuric acid (98%) and 20 ml phosphoric acid (85%) were mixed. 1.5 g of graphite flakes were added to the ice bath solution. 9 g of potassium permanganate was then slowly added to the mixture while stirring vigorously, maintaining a

temperature of 10±3 °C. After stirring for 15 minutes, the temperature was increased to 45±3 °C and stirring was continued for 24 hours. In the following step, the solution was added to a 0±3 °C, 200 ml H_2O_2 solution, which led to a rapid reaction and a color change of the mixture to brown. Finally, the mixture was washed with water, hydrochloric acid and ethanol. To prepare rGO, in a conventional synthesis method, a solution of NH_4OH was gradually added to a dispersion of GO (1 mg/ml) with constant stirring to ensure a stable pH of the solution of about 10. Hydrazine hydride was then added dropwise to the solution while maintaining the weight ratio of GO to hydrazine hydrate at 10:7. The resulting solution was subjected to treatment on an oil bath at constant temperature of 100±3°C for 1 hour with constant stirring. The rGO solution was then filtered and washed several times. To dope nitrogen into the rGO structure, a mixture of rGO and urea in a weight ratio of 1:25 was prepared and mixed with an agate mortar. The uniform mixture was then placed in a household microwave oven (1100 W) for 4 minutes. Fig. 1 Shows a schematic for synthesis of GO, rGO and N-rGO.

2-2- Synthesis of Li_2FeSiO_4/ N-rGO nanocomposite

A simple solid-state method was carried out to synthesize Li_2FeSiO_4 particles. Specifically, stochiometric amounts of fumed silica, iron oxide and lithium carbonate (0.98% purity, Merck) were ground with a mortar and pestle without additional purification. Typically, a certain amount of glucose was added to the mixture as a carbon source and reducing agent and mixed for 30 minutes to achieve a uniform mixture. Finally, the uniform mixture was calcined for 8 hours at 800 °C in a tube furnace under an Ar atmosphere with a controlled heating rate of 3 degrees/minute. The same procedures were followed for the synthesis of the Li_2FeSiO_4/N-rGO nanocomposite (denoted as LFS/NG) by adding 5, 10, and 15 wt% of the as-prepared N-rGO to the LFS precursors.

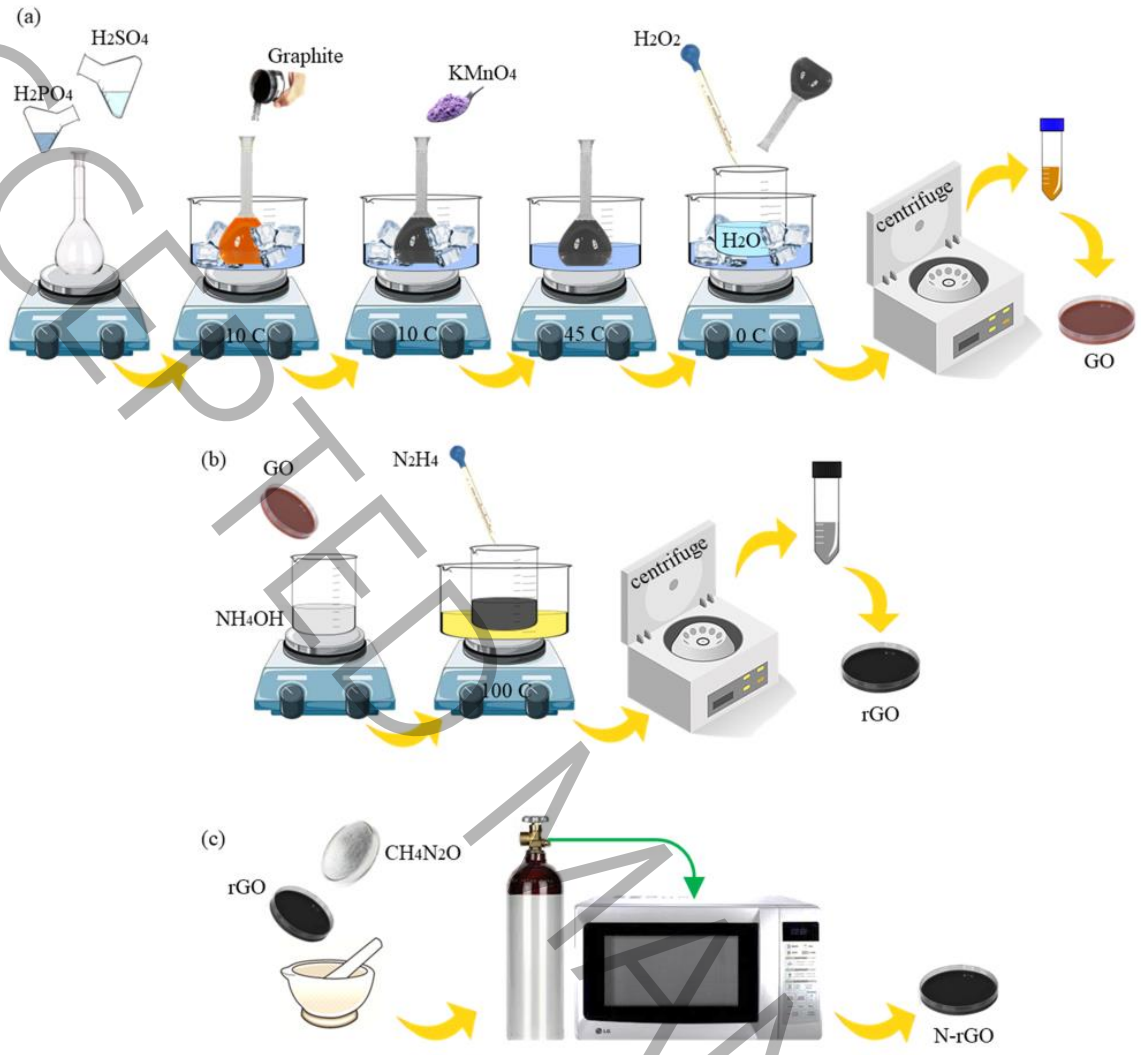

Fig. 1. Synthesis schematic of, a) GO, b) rGO, c) nitrogen-doped rGO.

2-3- Material characterization

All samples were removed for further characterization. Powder X-ray diffraction (XRD) patterns were created using the Philips PW1730 X-ray analyzer as a CuKα source (0.15405 nm). Fourier transform infrared spectroscopy (FTIR) was performed using the Thermo AVATAR spectrometer. RAMAN analysis was examined using Teksan TakRam N1-541 with 532 nm CW laser light as the excitation source. Moreover, dispersed powders were used for the field emission scanning electron microscopy (FESEM) and energy dispersive X-ray spectroscopy analyzer (EDS) with the TESCAN MIRA3 to study the morphological characterization, as well as for high resolution transmission electron microscopy (HRTEM)

on the EM 208S. To measure the surface area of the samples, the Brunauer-Emmett-Teller nitrogen adsorption-desorption (BET) were carried out using the BEL BELSORP MINI 2. Diffuse reflectance spectroscopy (DRS) and was used to estimate the bandgap of powders using the SCINCO S-4100 spectrometer. Finally, electrochemical impedance spectroscopy (EIS) measurement was performed with a frequency of 0.01-10^6 Hz and an AC amplitude of 10 mV using the BioLogic SP50c.

3. Result and discussion

The FTIR spectra of GO, rGO and N-rGO are shown in Fig. 2, respectively. As can be seen, several characteristic peaks associated with different functional groups are displayed. The broad peaks at 3446 cm^{-1} and 1625 cm^{-1} are related to OH groups of intercalated water in the composition and subsequently to the stretching and bending vibration of H-O-H's. Peaks at 1736 cm^{-1}, 1132 cm^{-1}, and 1014 cm^{-1} are also attributed to the carbonyl functional group of the C=O stretching vibration, the C=O bending vibration and the C-O stretching vibration. Compared to the spectra of rGO, the peak at 1736 cm^{-1} has disappeared. This proves the successful reduction of the carboxyl group in GO. The formation of aromatics can be seen at the peak at 1385 cm^{-1}. According to the spectra of NG, the peaks at 1049 cm^{-1} and 1120 cm^{-1} indicated C-N stretching. The stretching vibrations of C=C and C=N occur at 1576 cm^{-1}. The intensive broad peak at 1417 cm^{-1} is consistent with the C-H, O-H, and C-N bands. In addition, the peaks at 1697, 3216 and 3463 cm^{-1} are also attributed to C=O stretching, O-H stretching, and the N-H vibration sequentially. This allowed nitrogen atoms to be successfully doped into the structure of graphene layers [22, 25]. Fig. 3 shows RAMAN spectra of rGO and NG particles. At around 1373 cm^{-1} and 1588 cm^{-1}, two distinct peaks appear, which are assigned to the D and G bands. The G band is related to the E_{1g} mode and arises from the in-plane stretching vibration of graphite crystals. Moreover, all possible structural defects, such as poor crystallization, correspond to the D band. Such defects can be caused by doping elements in the structure of graphene (A_{1g} mode). Therefore, the higher intensity ratio of I_D/I_G means a higher proportion of the D-to-G band and more disorder points in the structure of NG. The I_D/I_G intensity ratio of NG (0.87) is higher

than that of rGO I_D/I_G (0.81) and has higher point defects such as pyrrole-N and pyridine-N in the graphene network [21, 22, 30].

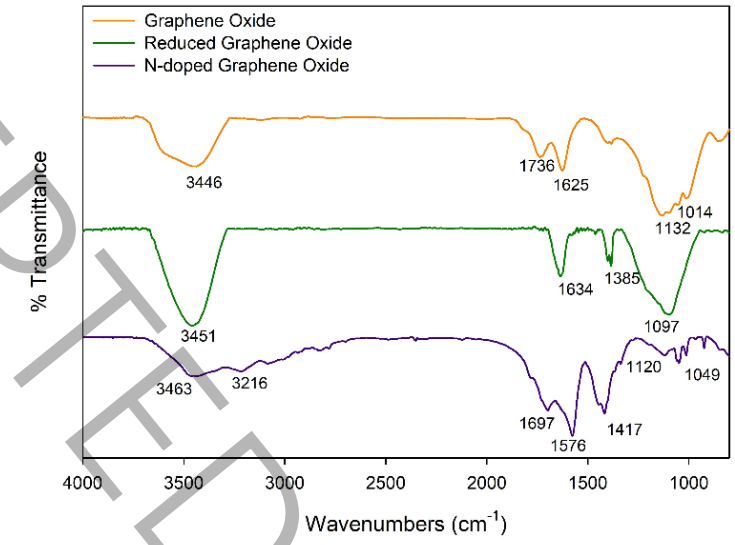

Fig. 2. The FTIR spectra of GO, rGO, and N-rGO particles

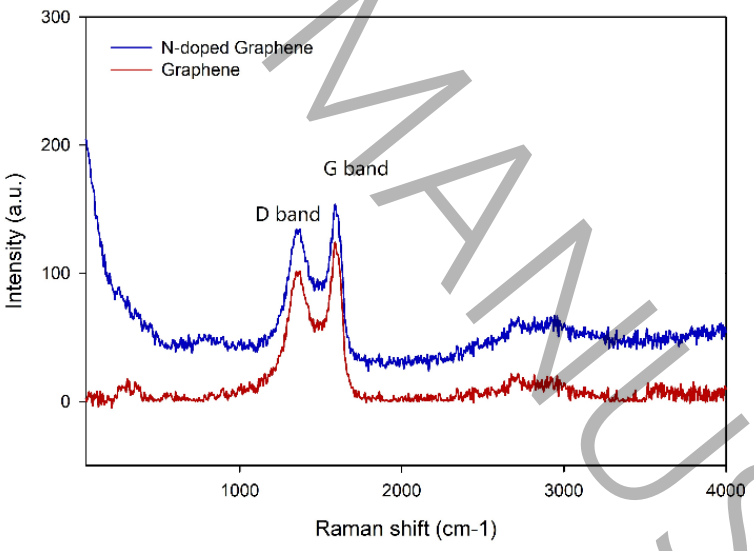

Fig. 3. The RAMAN spectra of rGO and N-rGO

Fig. 4 and Fig. 5 illustrate the morphological properties of rGO and N-rGO samples using FESEM and HRTEM images. According to the observations, all samples have a characteristic feature (an intricately folded sheet-like morphology with low contrast) indicating 50 nm thickness with few layers of rGO nanoparticles. The two-dimensional structure of rGO nanosheets gives rGO a significant surface area, making rGO an exceptional electrocatalytic material. The reduced contrast in N-rGO samples serves as an

indication of the reduced thickness of the plates (10 nm). Furthermore, the distinctly wrinkled morphology observed in N-rGO samples suggests potential contributing defects [30].

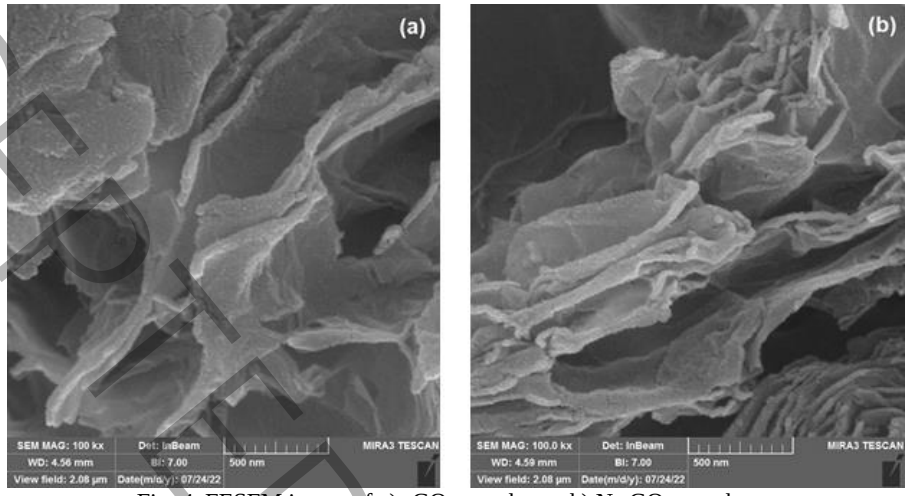

Fig. 4. FESEM image of a) rGO nanosheets, b) N-rGO nanosheets

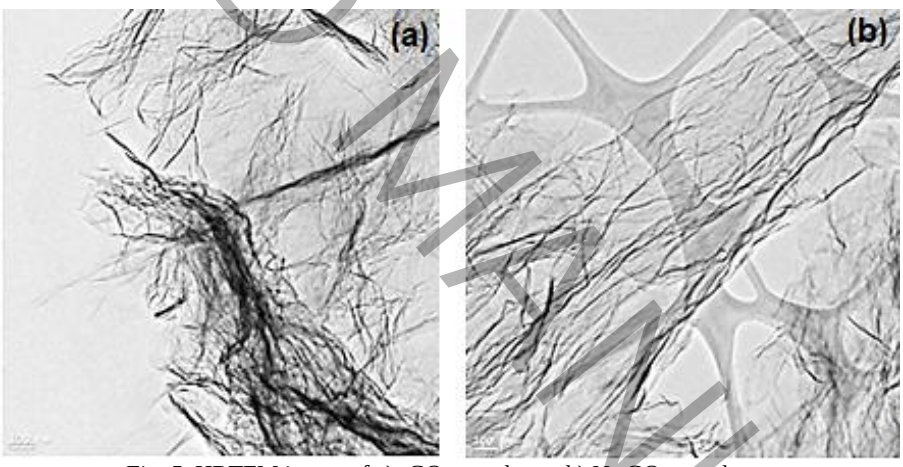

Fig. 5. HRTEM image of a) rGO nanosheets, b) N-rGO nanosheets

The XRD analysis shows the crystal structure of LFS and LFS/NG nanocomposite, as shown in Fig. 6 The peaks observed in both samples are consistent with the orthorhombic $Pmn2_1$, LFS structure (COD 96-702-1868) with Fe_3O_4 as an impurity. The XRD pattern of the LFS/NG nanocomposite is similar to the original LFS. It is worth mentioning that a structural change can be observed in the LFS during the charging and discharging process. When the crystal structure is monoclinic, it transitions from the initial monoclinic phase to a stable orthorhombic phase. Regardless of spatial phase, the monoclinic to orthorhombic transformation remains consistent. Therefore, the volume of the unit cell increases by about 1%, which can

have a negative impact on battery performance [31-33]. By performing a solid-state method that produces a stable orthorhombic pmn2_1-LFS structure, the expansion of the crystal structure and instability during battery charging/discharging is prevented. Moreover, Rietveld refinement was applied for both samples to extract crystal structure information such as lattice parameters. Crystallite size was measured by XRD patterns (Table 1) [34]. The addition of N-rGO as an LFS particle coating reduced the crystallite size by approximately 49 Å. This leads to a reduction in unite cell volume and a smaller particle size of LFS, resulting in a shorter diffusion path of lithium ions during battery charging/discharging. Comparing the phase analysis results, the purity of the original LFS phase and the LFS/NG nanocomposite is 98/48% and 98/47%, respectively, which is very acceptable for use as cathode material of LIBs.

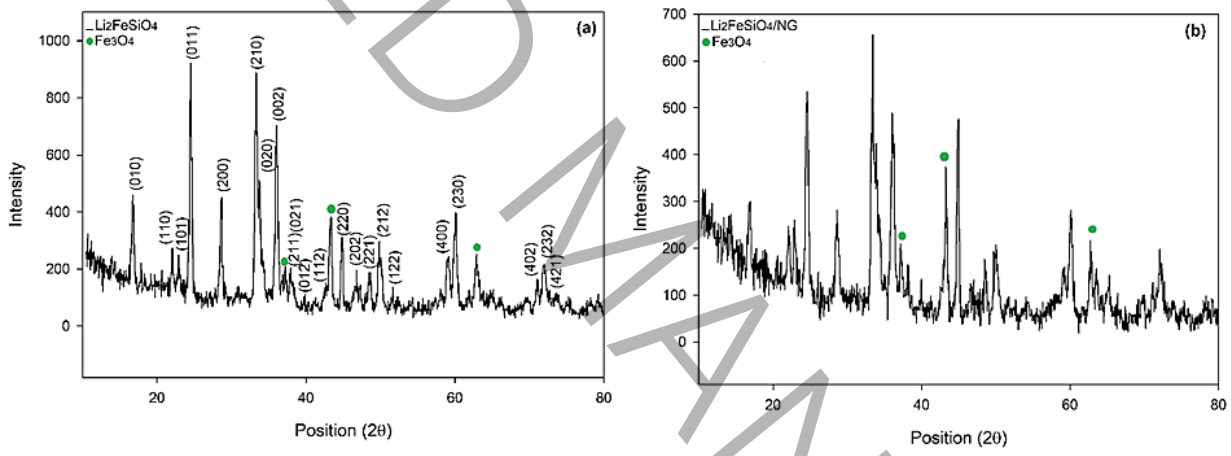

Fig. 6. X-ray diffraction patterns of a) LFS, b) LFS/NG

Table 1. Calculated lattice parameters, crystallite size, and unite cell volume of LFS and LFS/NG

sample	*Crystal lattice*	*Space phase*	*Phases* (%)		*a* (A)	*b* (A)	*c* (A)	*Crystallite size* (A)	*V* (A^3)
LFS	orthorhombic	Pmn2_1	LFS	98.48	6.25435	5.32373	5.00115	310	166.52
			Fe_3O_4	1.52					
LFS/5NG	orthorhombic	Pmn2_1	LFS	98.47	6.25876	5.31507	4.99664	261	166.21
			Fe_3O_4	1.53					

FESEM images of LFS and LFS/5wt%NG samples are shown in Fig. 7 Both samples consist of spherical particles. In contrast to LFS particles with a particle size of 400 nm, the LFS/5NG particles exhibit reduced agglomeration and particle size (300 nm), indicating the inhibitory effect of N-rGO on the agglomeration

of fine particles. These nanosheets of NG particles can be seen in the LFS/5NG image, which means that the LFS particles had a larger surface area. This can be demonstrated by a BET analyzer on both samples. The determined surface area is about 25.82 m^2/g and 32.80 m^2/g for LFS and the addition of only 5 wt% N-rGO to the LFS particles, respectively, suggesting that these materials are remarkable when are used as cathodes with active ingredients and electrolytes that interacted with the conductive material resulting in improved charging performance in lithium-ion batteries. The EDS mapping of LFS/5NG nanocomposites (Fig. 8) shows that all elements specifically C and N are evenly distributed throughout the sample, which obviously indicates the homogenous placement of LFS particles on N-rGO nanosheets.

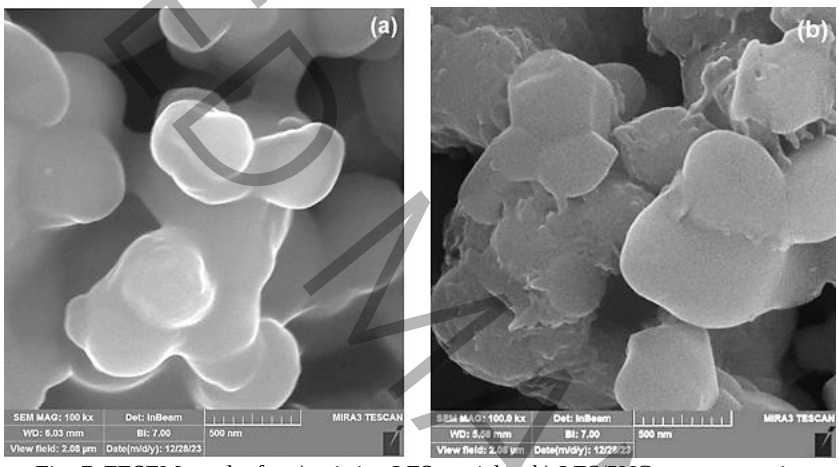

Fig. 7. FESEM results for a) pristine LFS particles, b) LFS/5NG nanocomposite

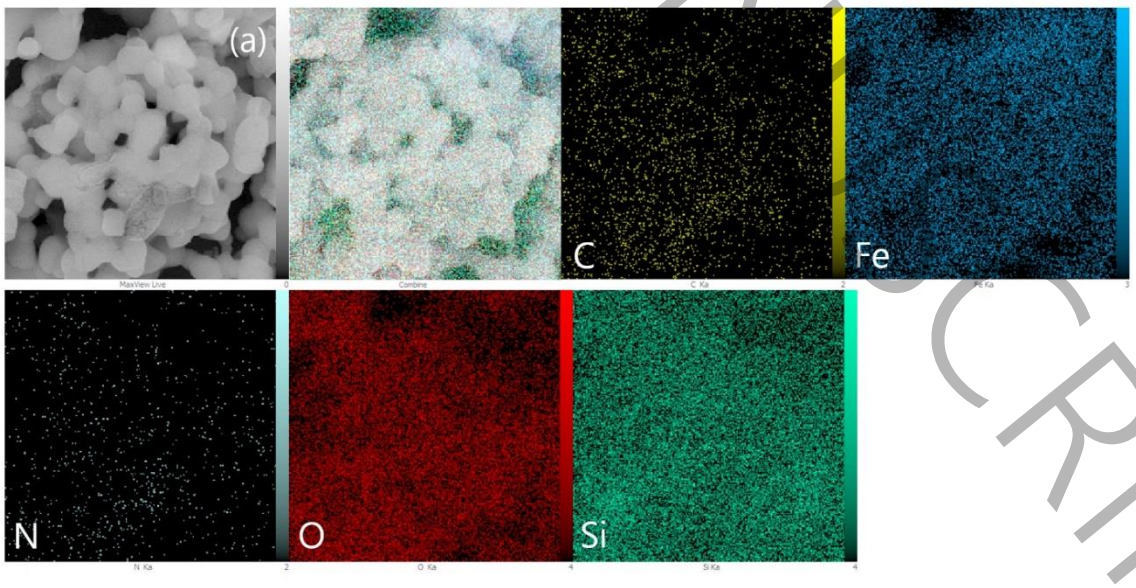

Fig. 8. The EDS mapping of LFS/5NG

The DRS analysis was performed to investigate the band gap of the LFS and LFS/NG. The optical absorption method showed favorable transmission. The direct bandgap was calculated using the Tauc relationship Eq. (1), where *h* is Planck's constant, *v* is the frequency of incident photos, *B* is a constant (band tailing parameter), and *m* is the index (2, 3, 1/2 or 1/3), which is indirectly permitted, indirectly prohibited, directly permitted and directly prohibited crossings [35].

$$\alpha h\nu = B(h\nu - Eg)^m \quad (1)$$

The band gap value was determined by plotting (*ahv*) versus *hv*, with the linear segment near the start of the absorption edge extrapolated to the energy axis, indicating a direct allowed transition for the system. The direct band gap of LFS and LFS/NG nanocomposites is shown in Fig. 9 In the absorption spectra (Fig. 10), pure nanocomposites with LFS/5 wt%NG, LFS/10 wt%NG, and LFS/15wt %NG exhibited wavelengths at 275 nm, 304 nm, 301 nm and 258 nm, respectively, which also illustrate the bandgap values for LFS with different concentrations of N-rGO. Table 2. Shows the measured bandgap values for all samples. The band gap increases from 2.80 eV to 3.17 eV, with the N-rGO concentration increasing from 5 wt% to 15 wt%. Reducing particle size contributes to a larger surface area to volume ratio, with surface atoms with lower coordination numbers and atomic interactions that result in an increase in the highest valance band energy and a decrease in the lowest unoccupied conduction band energy, consequently leading to an increased band gap. Accordingly, LFS/5NG with the narrowest band gap was chosen as the optimal active material.

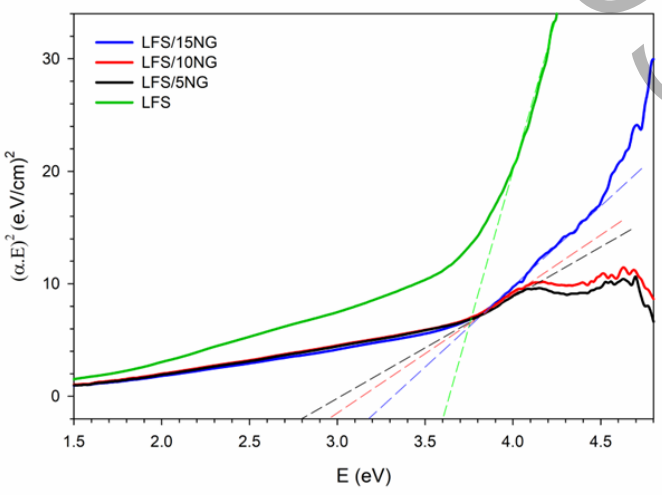

Fig. 9. Band gap energies of pristine LFS and LFS/NG nanocomposites

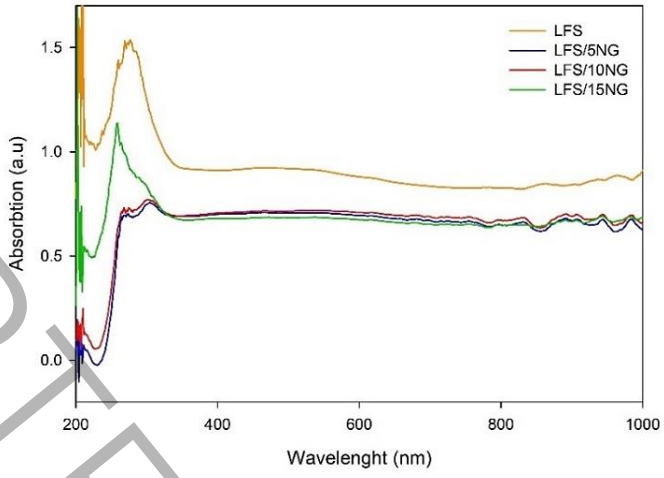

Fig. 10. Absorption spectra of LFS/NG nanocomposites in comparison with pristine LFS

Table 2. A comparison of the band gap energy values of as-prepared samples

As prepared samples	*The band gap energy* (eV)
LFS	3.58
LFS/5% NG	2.80
LFS/10% NG	2.98
LFS/15% NG	3.17

Fig. 11 shows the fitted Nyquist curve obtained by simulated EIS analysis for pristine LFS and LFS/5NG. The inset is the equivalent circuit that is used to fit the EIS data. The curve contains a semicircle at medium frequencies, which represent the charge transfer resistance (R_{CT}). The intersection of the Z' axis at high frequencies is the ohmic resistance (R_S). The 45-degree slope line or in other word, Warburg impedance is a factor that shows the diffusion condition on ionic conductivity of lithium ion in cathode material though a semi-infinite medium. To calculate the electronic conductivity, Eq. (2), is used [36-38].

$$\sigma = l / RA \qquad (2)$$

where *l* is the thickness, *R* the resistances and *A* the area or the direct contact of the cathode. Subsequently, the measured values of R_s for LFS and LFS/5NG are 7.07 Ω and 9.71 Ω. Also, R_{CT} for LFS and LFS/5NG are 582.6 Ω and 371.1 Ω. Therefore, an electronic conductivity of 2.21×10^{-5} s.cm^{-1} and 3.41×10^{-5} s.cm^{-1} are achieved for LFS and LFS/NG. by comparing charge transfer resistance and ohmic resistance of samples, both resistances of LFS/5NG decreased, due to the increase in specific surface area and the high elecrtocatalytic property of the nanocomposite caused by addition of 5 wt% rGO. Therefore, it is obvious that coating LFS particles with only 5 wt% N-rGO reduced the band gap energy value by about 0.78 eV, which corresponds to an increase in electrical conductivity of 54.31%. Table 3. shows a comparative analysis of the band gap values and electronic conductivity for different cathode samples of lithium batteries. The influence of bandgap energy on battery capacity and capability at different currents is comparable. As observed, the as-prepared LFS/5NG nanocomposite sample selected as the optimal cathodic active material can potentially be a candidate for improving battery performance.

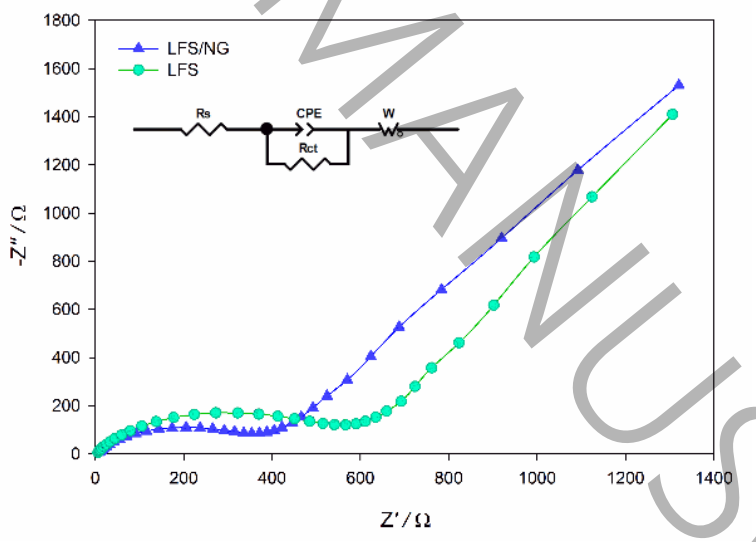

Fig 11. Nyquist plots for pristine LFS and LFS/5NG nanocomposite

Table 3. A comparison of measurements of other prepared LFS cathode material with this work

Samples	*Capacity* ($mAhg^{-1}$)	*Band gap* (eV)	*Electrical conductivity* ($S.cm^{-1}$)	*Ref.*
$Li_2Fe_{0.96}Y_{0.04}SiO_4/C$	150 at 0.2C	2.95	2.899×10^{-3}	[35]
$Li_2Fe_{0.98}Y_{0.02}SiO_4/C$	140 at 0.2C	3.04	2.152×10^{-3}	[35]
LFS monoclinic NPs*	140 at 0.2C	3.26	7.689×10^{-4}	[35]
LFS NPs	250 at 0.2C	2.13	-	[39]
LFS monoclinic NPs	133 at 0.1C	3.7	2.5×10^{-4}	[40]
LFS orthorhombic NPs	90 at 0.1C	3.1	-	[41]
LFS monoclinic	165 at 0.2C	3.3	-	[42]
LFS orthorhombic	-	3.58	2.21×10^{-5}	This work
LFS/5NG	-	2.8	3.41×10^{-5}	This work

*NPs: nanoparticles

4. The conclusion

LFS is a promising cathode material with significant theoretical capacity for lithium-ion batteries. This stable orthorhombic cathode active material was successfully synthesized by a simple solid-state technique with a high purity of 98%. Then, N-rGO with a multilayer structure was fabricated as a coating of LFS sample using a domestic microwave method. Nitrogen atoms could be successfully localized in the rGO structure and the defect sites were leveled, resulting in better electrocatalyst properties. Furthermore, N-rGO reduced the accumulation of LFS particles as well as their size and increased the surface area of the samples by about 27%. The study investigated the influence of different percentages of N-rGO coating on the electrical conductivity of the LFS by comparing their bandgap energy values. Coating LFS particles with 5 %wt NG resulted in a decrease in the energy of the bandgap value by about 0.78 eV and an increase in electrical conductivity by 54.31%. This suggests that LFS with a 5% N-rGO coating could be a candidate as an active material for lithium-ion batteries.

5. References

[1] T.ZM. Bawm, A.R.Md. Harunur Rashid, M. Hasanuzzaman, Effects of Doping/Co-Doping on Li2FeSiO4 Cathode Material for Lithium-Ion Batteries: A Review, Encyclopedia of Materials: Electronics, 3 (2023) 381-391.

[2] T. Muthu Muniyandi, S. Balamurugan, N. Naresh, I. Prakash, R. Venkatesh, U. Deshpande, N. Satyanarayana, Li2FeSiO4/C aerogel: A promising nanostructured cathode material for lithium-ion battery applications, Journal of Alloys and Compounds, 887 (2021) 161341.

[3] X. Bi, L. Chang. Sh. Luo, Sh. Cao, A. Wei, W. Yang, J. Liu, F. Zhang, The recent progress of Li2FeSiO4 as a poly-anionic cathode material for lithium-ion batteries, Energe Reaserch, 46 (2021) 5373–5398.

[4] F. Zheng, Q. Lin, S. Wu, Z.-z. Zhu, Influence of the Fe-Si-O framework in crystal structure on the phase stability and electrochemical performance of Li2FeSiO4 cathode, Solid State Ionics, 356 (2020) 115436.

[5] H. Kageyama, Y. Hashimoto, Y. Oaki, H. Imai, Six-armed twin crystals composed of lithium iron silicate nanoplates and their electrochemical properties, CrystEngComm, 17(44) (2015) 8486-8491.

[6] A. Nytén, A. Abouimrane, M. Armand, T. Gustafsson, J.O. Thomas, Electrochemical performance of Li2FeSiO4 as a new Li-battery cathode material, Electrochemistry communications, 7(2) (2005) 156-160.

[7] X.B. Longjiao Chang, Shaohua Luo, Wei Yang, Anlu Wei, n Yang, Jianan Liu, Insight into the high-efficiency separation of Si element from low-grade laterite nickel ore and the preparation of Li2FeSiO4/C cathode materials for lithium-ion batteries, Journal of Alloys and Compounds, 937(168357) (2023).

[8] H.C. Yutian Yang, Rihuang Nie, Cheng Li, Shuangwu Xu, Mengcheng Zhou, Xinyu Zhang, Hongming Zhou, Using the synergistic effect of co-doping to engineer magnesium and chlorine co-doping to improve the electrochemical performance of Li2FeSiO4/C cathodes, Journal of Alloys and Compounds, 935(167958) (2023).

[9] S. Chakrabarti, A.K. Thakur, K. Biswas, Effect of Ti modification on Structural, Electronic and Electrochemical properties of Li 2 FeSiO 4 —A DFT study using FPLAPW approach, Electrochimica Acta, 236 (2017) 288-296.

[10] H. Li, Y. Li, X. Cheng, C. Gong, Hollow Hemispherical Lithium Iron Silicate Synthesized by an Ascorbic Acid-Assisted Hydrothermal Method as a Cathode Material for Li Ion Batteries, Materials (Basel), 15(10) (2022).

[11] S. Yi, J. Moon, M. Cho, K. Cho, Ab-initio design of novel cathode material LiFeP1-SiO4 for rechargeable Li-ion batteries, Electrochimica Acta, 313 (2019) 70-78.

[12] Y.L. Xiaoying Luo, Xuan Cheng, Mechanistic study in sulfur-carbon co-modification on Li2FeSiO4 for lithium-ion batteries, Ceramics International, 49 (2023) 27277–27287.

[13] H. Qiu, D. Jin, C. Wang, G. Chen, L. Wang, H. Yue, D. Zhang, Design of Li2FeSiO4 cathode material for enhanced lithium-ion storage performance, Chemical Engineering Journal, 379 (2020) 122329.

[14] K. Pushnitsa, P. Novikov, A. Popovich, Q. Wang, Synthesis of Li2FeSiO4/C composite cathode material for Li-ion batteries and influence of dispersion effect on electrochemical characteristics, Materials Today: Proceedings, 30 (2020) 773-777.

[15] P. Vajeeston, Ionic conductivity enhancement by particle size reduction in Li2FeSiO4, Materials Letters, 218 (2018) 313-316.

[16] B. Shen, J. Zeng, N. Fu, X. Wang, Zh. Yong, High reversible capacity silicon anode by segregated graphene-carbon nanotube networks for lithium ion half/full batteries, Energy Storage, 55 (2022) 105767.

[17] T. Liu, Y. Liu, Y. Yu, Y. Ren, C. Sun, Y. Liu, J. Xu, C. Liu, Z. Yang, W. Lu, P. Ferreira, Z. Chao, J. Xie, Approaching theoretical specific capacity of iron-rich lithium iron silicate using graphene-incorporation and fluorine-doping, Journal of Materials Chemistry A, 10(8) (2022) 4006-4014.

[18] W. Zhang, W. Shao, B. Zhao, K. Dai, Review—Research Progress of Li2FeSiO4 Cathode Materials for Lithium-Ion Batteries, Journal of The Electrochemical Society, 169(7) (2022) 070526.

[19] J. Yang, X. Kang, D. He, A. Zheng, M. Pan, S. Mu, Graphene activated 3D-hierarchical flower-like Li2FeSiO4 for high-performance lithium-ion batteries, Journal of Materials Chemistry A, 3(32) (2015) 16567-16573.

[20] J. Yang, L. Hu, J. Zheng, D. He, L. Tian, Sh. Mu, F. Pan, Li2FeSiO4 nanorods bonded with graphene for high performance batteries, Materials Chemistry A, 3 (2015) 9601–9608.

[21] L.L. Zhang, S. Duan, X.L. Yang, G. Peng, G. Liang, Y.H. Huang, Y. Jiang, S.B. Ni, M. Li, Reduced graphene oxide modified Li2FeSiO4/C composite with enhanced electrochemical performance as cathode material for lithium ion batteries, ACS Appl Mater Interfaces, 5(23) (2013) 12304-12309.

[22] Y. Shang, H. Xu, M. Li, G. Zhang, Preparation of N-Doped Graphene by Hydrothermal Method and Interpretation of N-Doped Mechanism, Nano, 12(02) (2017) 1750018.

[23] X. Wang, C. Qing, Q. Zhang, W. Fan, X. Huang, B. Yang, J. Cui, Facile synthesis and enhanced electrochemical performance of Li2FeSiO4/C/reduced graphene oxide nanocomposites, Electrochimica Acta, 134 (2014) 371-376.

[24] Z. Liu, Q. Wang, B. Zhang, T. Wu, Y. Li, Efficient Removal of Bisphenol A Using Nitrogen-Doped Graphene-Like Plates from Green Petroleum Coke, Molecules, 25(15) (2020) 3543.

[25] D.R.A.B. Alyaa. K. Mageed, A. Salmiaton, Shamsul Izhar, Musab Abdul Razak, H.M.Yusoff, F.M. Yasin, Suryani Kamarudin, Preparation and Characterization of Nitrogen Doped Reduced Graphene Oxide Sheet, nternational Journal of Applied Chemistry, 12 (2016) 104-108.

[26] H. Aghajani, A.T. Tabrizi, R. Ghorbani, S. Behrangi, M. Stupavska, N. Abdian, Evaluation of electrochemical hydrogen storage capability of three-dimensional nano-structured nitrogen-doped graphene, Journal of Alloys and Compounds, 906 (2022) 164284.

[27] X.D. H. Gao, Q. Wu, Z. Gao, Sh. Lou, Y. Zhao, Improved capacity and cycling stability of Li2FeSiO4 nanocrystalline induced by nitrogen-doped carbon coating, Solid State Electrochemistry, 25 (2021) 1679–1689.

[28] H. Gao, Q. Wu, M. Guo, S. Yang, Y. Zhao, Y.-U. Kwon, Rationally fabricating nitrogen-doped carbon coated nanocrystalline Li2FeSiO4@N-C with excellent Li-ion battery performances, Electrochimica Acta, 318 (2019) 720-729.

[29] Z. Dong Peng, Y. Bing Cao, G. Rong Hu, K. Du, X. Guang Gao, Z. Wei Xiao, Microwave synthesis of Li2FeSiO4 cathode materials for lithium-ion batteries, Chinese Chemical Letters, 20(8) (2009) 1000-1004.

[30] M. Rahsepar, F. Foroughi, H. Kim, A new enzyme-free biosensor based on nitrogen-doped graphene with high sensing performance for electrochemical detection of glucose at biological pH value, Sensors and Actuators B: Chemical, 282 (2019) 322-330.

[31] Y. Zeng, H.-C. Chiu, M. Rasool, N. Brodusch, R. Gauvin, D.-T. Jiang, D.H. Ryan, K. Zaghib, G.P. Demopoulos, Hydrothermal crystallization of Pmn21 Li2FeSiO4 hollow mesocrystals for Li-ion cathode application, Chemical Engineering Journal, 359 (2019) 1592-1602.

[32] X. Lu, H.-C. Chiu, Z. Arthur, J. Zhou, J. Wang, N. Chen, D.-T. Jiang, K. Zaghib, G.P. Demopoulos, Li-ion storage dynamics in metastable nanostructured Li2FeSiO4 cathode: Antisite-induced phase transition and lattice oxygen participation, Journal of Power Sources, 329 (2016) 355-363.

[33] T. Masese, C. Tassel, Y. Orikasa, Y. Koyama, H. Arai, N. Hayashi, J. Kim, T. Mori, K. Yamamoto, Y. Kobayashi, H. Kageyama, Z. Ogumi, Y. Uchimoto, Crystal Structural Changes and Charge Compensation Mechanism during Two Lithium Extraction/Insertion between Li2FeSiO4 and FeSiO4, The Journal of Physical Chemistry C, 119(19) (2015) 10206-10211.

[34] S. Emami, H. Aghajani, A.T. Tabrizi, Sustainable Oxygen-Free Copper Powder Production Method from Wastes, Journal of Sustainable Metallurgy, 9(4) (2023) 1803-1809.

[35] H. Qiu, H. Yue, T. Zhang, Y. Ju, Y. Zhang, Z. Guo, C. Wang, G. Chen, Y. Wei, D. Zhang, Enhanced Electrochemical Performance of Li 2 FeSiO 4 /C Positive Electrodes for Lithium-Ion Batteries via Yttrium Doping, Electrochimica Acta, 188 (2016) 636-644.

[36] R. Tan, J. Yang, J. Zheng, K. Wang, L. Lin, S. Ji, J. Liu, F. Pan, Fast rechargeable all-solid-state lithium ion batteries with high capacity based on nano-sized Li2FeSiO4 cathode by tuning temperature, Nano Energy, 16 (2015) 112-121.

[37] L. Liu, P. Wang, J. Li, G. Shi, L. Ma, J. Zhao, H. An, Hydrothermal preparation and intrinsic transport properties of nanoscale Li2FeSiO4, Solid State Ionics, 320 (2018) 353-359.

[38] P. Sivaraj, B. Nalini, K.P. Abhilash, D. Lakshmi, P. Christopher Selvin, P. Balraju, Study on the influences of calcination temperature on structure and its electrochemical performance of Li2FeSiO4/C nano cathode for Lithium Ion Batteries, Journal of Alloys and Compounds, 740 (2018) 1116-1124.

[39] J. Yang, J. Zheng, X. Kang, G. Teng, L. Hu, R. Tan, K. Wang, X. Song, M. Xu, S. Mu, F. Pan, Tuning structural stability and lithium-storage properties by d -orbital hybridization substitution in full tetrahedron Li 2 FeSiO 4 nanocrystal, Nano Energy, 20 (2016) 117-125.

[40] L.-L. Zhang, H.-B. Sun, X.-L. Yang, Y.-W. Wen, Y.-H. Huang, M. Li, G. Peng, H.-C. Tao, S.-B. Ni, G. Liang, Study on electrochemical performance and mechanism of V-doped Li2FeSiO4 cathode material for Li-ion batteries, Electrochimica Acta, 152 (2015) 496-504.

[41] Y. Zeng, H.-C. Chiu, B. Ouyang, K. Zaghib, G.P. Demopoulos, Defect Engineering of Iron-Rich Orthosilicate Cathode Materials with Enhanced Lithium-Ion Intercalation Capacity and Kinetics, ACS Applied Energy Materials, 3(1) (2019) 675-686.

[42] L. Li, E. Han, M. Jiao, Y. Zhang, X. Yang, W. Yuan, The effect of Ag or Zn composite on the electrochemical performance of Li2FeSiO4 cathode materials, Ionics, 26(6) (2020) 2727-2736.